This manuscript was accepted by Rev. Sci.Instrum. Click here to see the version of record.

Design and implementation of a low temperature, inductance based high frequency alternating current susceptometer

E. Riordan,[1] J. Blomgren,[2] C. Jonasson,[2] F. Ahrentorp,[2] C. Johansson,[2] D. Margineda,[1] A. Elfassi,[3] S. Michel,[3] F. Dell'ova,[3] G. M. Klemencic,[1] and S. R. Giblin[1, a)]

[1)] *Department of Physics & Astronomy, Cardiff University, Cardiff, CF24 3AA, United Kingdom*

[2)] *RISE Acreo, Arvid Hedvalls Backe 4, Box 53071, SE-400 14, Göteborg, Sweden*

[3)] *INSA, Institut National des Sciences Appliques, TOULOUSE, 135 Avenue de Rangueil, 31077 Toulouse Cedex 4, France*

We report on the implementation of an induction based, low temperature, high frequency ac susceptometer capable of measuring at frequencies up to 3.5 MHz and at temperatures between 2 K and 300 K. Careful balancing of the detection coils and calibration allow a sample magnetic moment resolution of 5×10^{-10} Am^2 at 1 MHz. We discuss the design and characterization of the susceptometer, and explain the calibration process. We also include some example measurements on the spin ice material $CdEr_2S_4$ and iron oxide based nanoparticles to illustrate functionality.

I. INTRODUCTION

In ac susceptibility measurements a sinusoidal ac magnetic field, H(t), with a small field amplitude is applied to the sample and the dynamic magnetization, M(t), of the sample is measured thus allowing the ac susceptibility, $\chi = \partial \mathrm{M(t)}/\partial \mathrm{H(t)}$, to be determined[1–3]. M(t) is given by $\mu(t)/v$ or $\mu(t)/m$ for volume or mass magnetization respectively, where $\mu(t)$ is the sample's magnetic moment, v is the sample volume and m is the sample mass. The ac susceptibility can be represented as a frequency dependent complex magnetic susceptibility: $\chi(\omega) = \chi'(\omega) - i\chi''(\omega)$. $\chi'(\omega)$ is in-phase with the excitation ac-field whilst the out-of-phase component, $\chi''(\omega)$, (with a phase angle at 90° with respect to the applied ac magnetic field) represents energy losses from the excitation field to the sample. Throughout this paper we use mass magnetization and mass susceptibility which we denote with the subscript M_m and χ_m.

Ac susceptibility measurements based on the induction technique[4] have allowed a wide variety of physical phenomena to be probed. This has included the application of the technique to thermometry[5], superconductivity[6], magnetic nanoparticles[7], and magnetic glasses[8]. Dynamical processes, such as magnetic relaxation can be measured, where the out-of-phase component of the susceptibility exhibits a relaxation peak at a frequency corresponding to a characteristic relaxation time. Magnetic relaxation dependent processes in magnetic nanoparticle systems include the intrinsic Néel relaxation and extrinsic Brownian relaxation which can demonstrate magnetic relaxation properties from a few Hz to the MHz range[9]. Induction based ac susceptometers capable of measuring at low temperatures are generally limited to the kHz range. Those ac susceptometers that allow measurement into the MHz range are currently limited to room temperature[10]. Other techniques have been used to measure ac susceptibility at low temperatures and high frequencies, including the use of resonant circuits[11] and the tunnel diode oscillator technique[12], which require long measurement times for multiple frequencies. Toroidal based systems are capable of measuring into the GHz range but are limited by low sensitivity and difficulties in mounting of the sample[13–15]. Micro-SQUID systems suitable for microscopic samples have also worked at high frequencies[16]. The system discussed in this paper is a versatile induction based system allowing both the in-phase and out-of-phase components of the susceptibility to be easily separated up to the MHz regime for bulk samples; moreover the system works in commercial cryostats allowing temperatures from 2-300 K and dc magnetic fields to be swept from 0-9 T. This enables measurement of relaxation effects in samples across a varied range of phase space previously only accessible by central facility techniques such as muon spin rotation which requires a particle accelerator. This system will have useful applications in many areas of physics including frustrated magnetism, superconductivity, as well as magnetic nanoparticles, which can be used for biomedical applications.

II. PRINCIPLES OF INDUCTION BASED AC SUSCEPTOMETRY

Induction based ac susceptometers consist of two circuits: an excitation circuit and detection circuit. In a first order gradiometer (such as our susceptometer) the detection circuit consists of two in-series counter-wound coils connected to a lock-in amplifier. The detection coils are counter-wound to ensure a minimal response to the application of any external field. More complex second order coils can be designed, however for systems at high frequency the inductive and capacitive response is of more concern. During an ac susceptibility measurement a sinusoidally oscillating magnetic field is applied to the region of the detection coils by the excitation coil. The sample is first placed in the center of one of the detection coils, changing the magnetic flux through it and therefore changing the voltage amplitude detected by the lock-in amplifier. The sample is then moved to the center of the second detection coil causing a voltage change of the opposite sign. The frequency of the excitation field

[a)] giblinsr@cardiff.ac.uk

does not change during this process. The difference between the measured voltage in the upper and lower coils can then be related to the susceptibility by

$$\Delta V = \mu_0 \omega \alpha N A i M_{m,0} = \mu_0 \omega \alpha N A H_0 (\chi''_m + i\chi'_m) \quad (1)$$

where, $\Delta V = V_U - V_L$ (V_U and V_L are measured voltage amplitudes when the sample is in the upper and lower detection coil respectively), $M_{m,0}$ is the amplitude of the mass magnetization of the sample, N is the number of turns in the detection coils, A is the cross sectional area of the coils, i is the imaginary unit ($i^2 = -1$), ω is the angular frequency being measured ($\omega = 2\pi f$ where f is the excitation frequency), H_0 is the amplitude of the excitation field, α is a complex coupling factor that is dependent on the coil geometry and sample properties, χ'_m and χ''_m are the in-phase and out-of-phase components of the mass susceptibility respectively, and μ_0 is the permeability of free space. Finding α experimentally is required to calibrate an instrument and the method for this particular instrument is outlined in section IV using a process that requires a sample that has a known in- and out-of-phase component of its ac susceptibility; historically Dy_2O_3 meets the requirement for the frequency range of interest[17].

A major difficulty in achieving high frequencies in induction based ac susceptometers is reducing the parasitic capacitance and inductance due to the windings of the excitation and detection coils. This is necessary for two reasons. Firstly, the parasitic capacitance and inductance give a resonance at a specific frequency that must be well above the measureable frequency range. Secondly, the field produced by the excitation coil is directly proportional to the current through it, so if the impedance (due to coil reactance) increases then the field amplitude decreases, a smaller field means a smaller detectable moment for a given sample susceptibility.

III. INTERFACE & COIL SET

Our ac susceptometer is designed for use in a Quantum Design physical property measurement system (QD-PPMS). Full automation of the ac susceptibility measurement, including control of the temperature and dc magnetic field provided by the QD-PPMS, was achieved using a Labview interface. Although the temperature stability of the sample relies upon exchange gas, careful calibration is required to ensure no parasitic Joule heating effect; this can be measured by knowing the temperature dependent response of known samples and careful monitoring and calibration of the system with thermometers in the heat exchanger and the neck of the variable temperature insert (VTI) of the cryostat. The neck thermometer in the wall of the VTI also allows the ability to monitor effective eddy current heating in the wall of the variable temperature insert from the excitation field. A Stanford Research Systems DS345 signal generator is used to drive the excitation coil and a Stanford Research Systems SR844 or SR830 lock-in amplifiers (the SR830 with a 50 Ω terminator) are used for the phase sensitive detection. The SR844 is capable of measuring well beyond the upper frequency limit of our system, but limits the lowest accessible frequency to 25 kHz. The SR830 can measure well below the lower limit of our system, but limits the maximum frequency to 102 kHz. The sample is moved between the detection coils using an Accu-Glass 2" linear actuator mounted at the top of the sample space. Samples are mounted in plastic drinking straws which fix to the end of a long carbon fibre rod that attaches to the actuator magnetically. Figure 1 shows an experimental diagram of the hardware.

Our susceptometer is similar to the Dynomag HF (High Frequency) system[10], which allows measurements up to 10 MHz at room temperature. The ac susceptometer presented in this paper consists of a NbTi excitation coil with N=24 turns, wound in a double layered helix to minimize parasitic capacitance. Two N=2 turn shim coils are used at both ends to achieve a field that is uniform along the axis of the excitation coil. NbTi was chosen to reduce parasitic heating below the superconducting transition ($T_c = 9.8K$). The detection coils consist of two in-series counter-wound copper coils of N=15 turns each.

The excitation field was calibrated using a longitudinal Hall probe with a dc current applied to the coil, from this the field produced per unit applied current (B/I) can be calculated. B/I can then be used to measure the response of the coil as a function of frequency for an ac current. Figure 2a displays the result of these measurements, resulting in a B/I value of (0.358±0.008) mT/A. The measured excitation field is in agreement with the fit within measurement error at large currents. The frequency characteristics of the current through the excitation coil were measured using a custom made analogue differential input amplifier and an oscilloscope. It is then trivial to calculate how the field amplitude behaves with frequency, the results of which are shown in figure 2b. A 90.9 Ω resistor is placed in series with the excitation coil when it is in the superconducting phase in order to achieve a known excitation field. It is also possible to remove this resistor to apply a much larger excitation field if required but that will be limited by the 50 Ω series impedance of the signal generator.

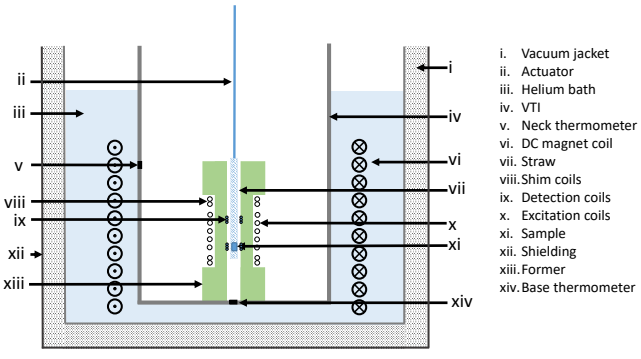

Figure 1: *Diagram of the experimental system including the Helium bath cryostat and the VTI. The DC magnet is in the Helium bath with the AC magnet and detection coils in the VTI.*

To reduce the ringing of the detection coil due to the coil's LC-resonance, it is common practice to put damp-

ing resistances in parallel with each counter-wound detection coil in the detection circuit. In the current setup the detection coil is connected directly to a lockin amplifier and hence the damping can alternatively be achieved by using a 50 Ω input impedance on the lock-in amplifier. Our system is capable of measuring up to 3.5 MHz, however the minimum detectable ac susceptibility increases above 1.5 MHz due to the increasing excitation coil impedance reducing the excitation current. The inset of Figure 2b shows the resonance of the excitation and detection coil for the circuit clearly demonstrating the limits of the linear response of the system. This response is temperature independent and the detection circuit has a capacitance and inductance of 4.79 μH and 82 pF respectively.

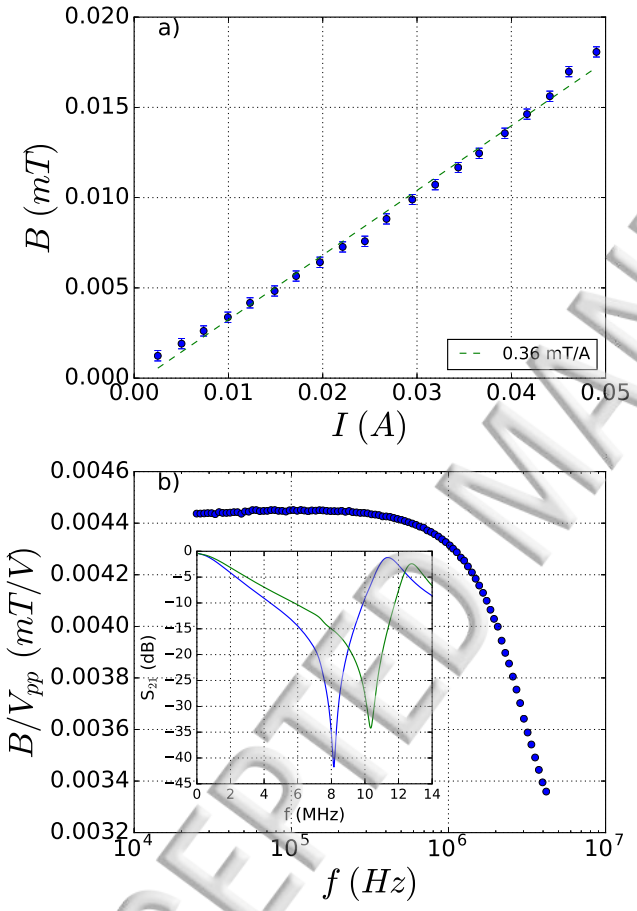

Figure 2: *a) Magnetic flux in the center of the coil set as measured by a longitudinal hall probe against applied dc current, with the linear fit showing the B/I vlaue. b) Frequency dependence of the excitation field. The inset shows transmission measurements of the coil resonances for the excitation (green) and detection coil (blue).*

IV. MEASUREMENT PROCESS & CALIBRATION

To perform any measurement with the susceptometer it is first necessary to locate the sample relative to the detection coils. This is performed by moving the sample through the entire range available to the actuator and continually recording on the lock-in amplifier. As the sample moves the changing flux in the detection circuit is measured by the lock-in as a voltage, therefore mapping the oscillating dipole moment of the sample to voltage as a function of distance along the coil axis, z. The induced voltage amplitude, $|V(z)|$, can be represented by;

$$|V(z)| = F\frac{{A_1}^2}{({A_1}^2+(z-z_1)^2)^{3/2}} - F\frac{{A_2}^2}{({A_2}^2+(z-z_2)^2)^{3/2}} + C \quad (2)$$

where A_1 and A_2, represent the radius of each detection coil, z is the sample position along the coil axis, F is a constant relating the flux amplitude (from the sample) cutting the gradiometer to the induced voltage amplitude and C is a background voltage term. z_1 and z_2 are the positions of the upper and lower coils respectively. An example trace and fit are shown in figure 3 showing the coil locations at $z_1 = 0.0098$ m and $z_2 = 0.0374$ m. The peaks in the location scan represent the position of the sample with respect to the first order gradiometer, an essential component in the calibration of the system because the absolute magnitude of the measured susceptibility depends upon correct placement of the measurement sample relative to the detection coils. The position of the sample is monitored by a linear resistor on the sample actuator accurate to within 0.1mm, this level of accuracy is necessary because a sample position error of 0.5 mm in one coil can give a 1 % error in the recorded voltage.

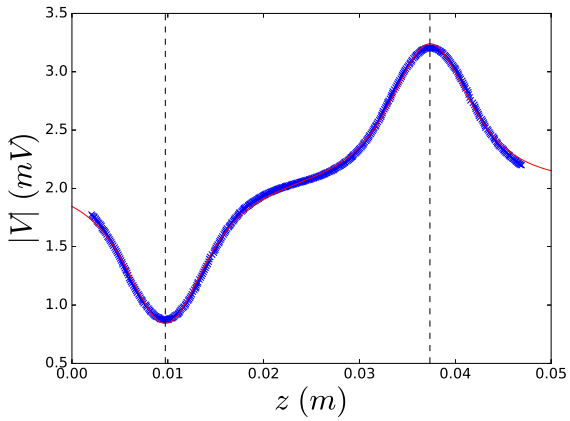

Figure 3: *Magnitude of the raw voltage recorded on the lock-in amplifier against the sample position in the coil set. Blue crosses show the raw data and the red line is a fit to equation 2. Vertical dashed lines indicate detection coil centers z_1 and z_2.*

Two further processes are required for the calibration. The first involves a simple background measurement, where an empty sample holder is moved between the detection coils and the voltages are measured in the upper and lower coils. The difference ΔV_b is subtracted from the voltages recorded during a measurement. The second is a gain and phase calibration that is used to determine an appropriate scaling factor for the measured voltage and to account for frequency dependent phase shifts introduced by the complex impedance of the equipment.

A sample with a well known and frequency independent susceptibility, χ_{cal}, is required and then a complex calibration factor, G, is chosen such that the observed ΔV results in χ_{cal} at each frequency. Here we have used mass susceptibility $\chi_{m,cal}$ but a similar process can be done using volume susceptibility. In more detail, G can be written as:

$$G = \frac{\chi_{m,cal} m_{cal} H 2\pi f}{\Delta V_{cal} - \Delta V_b} \tag{3}$$

where m_{cal} is the mass of the calibration sample, H is the applied magnetic field, ΔV_{cal} is the voltage difference measured from the calibration sample. An example of the calibration factor in polar coordinates is shown in Figure 4, where gain is the amplitude of G with units $\mathrm{Am^2V^{-1}s^{-1}}$. When a sample is measured, the calibration factor is used to convert the measured voltage difference ΔV_s to a sample mass susceptibility $\chi_{m,s}$:

$$\chi_{m,s} = \frac{G(\Delta V_s - \Delta V_b)}{m_s H 2\pi f} \tag{4}$$

where m_s is the sample mass. Alternatively, the susceptibility of the sample can be expressed as a volume susceptibility, $\chi_{V,s}$, by dividing with the sample volume instead of the sample mass. G is related to α in equation 1 by: $G = -im_s/(\mu_0 \alpha N A)$.

A key consideration of the system is the response over the entire temperature range. We have used two well understood samples to cover a large temperature range; Dy_2O_3, a paramagnetic material for the high temperature regime and Pb, a superconductor at low temperature. It is impractical to calibrate at every temperature and so calibrations are generally only performed at 2 K for the Pb and 100 K for Dy_2O_3 which are then used for measurements across a broad temperature range. Examples of gain and phase calibrations are shown in figures 4a and b respectively across a range of temperature and frequency. Both calibration samples produce similar phase corrections (some difference is expected because the excitation coil is superconducting below 9.8 K) and near identical amplitudes of G.

An empty sample holder was measured across the full temperature range to check for an inherent temperature dependence of the system that would have to be accounted for in measurements. Calibration was performed as described above (at 100 K) and the background voltage amplitude was measured from 10K-266 K as shown in figure 5. The amplitude of the excitation field is known to vary according to the temperature dependence of the resistance of NbTi wire and so this has been corrected for in figure 5 by scaling the detected voltage appropriately. As shown in figure 5, a linear least squares fit has found a gradient of $(-3.79 \pm 5.27) \times 10^{-10}\ V/K$ indicating a very weak to non existent relationship between temperature and detected voltage, as any change is within the background noise. The voltages shown in figure 5 are two orders of magnitude smaller than typical measurement voltages.

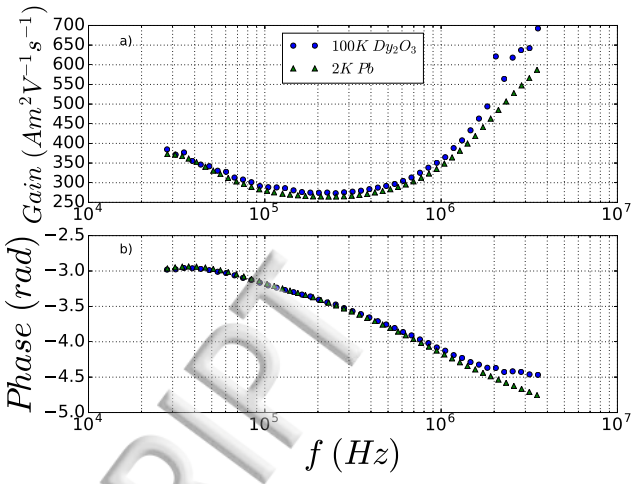

Figure 4: *a) Example gain calibrations at different frequencies. b) Example of phase corrections at different frequencies. In both panels blue circles show a calibration taken at 100 K and the green triangles show a calibration at 2 K.*

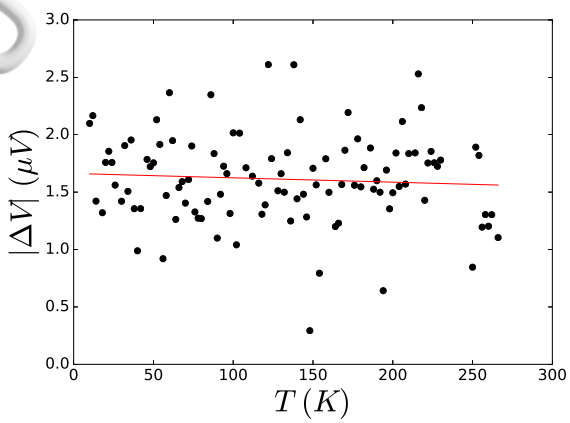

Figure 5: *Magnitude of the measured complex voltage against temperature, as detected by the lock-in for the case of an empty sample holder at 1 MHz. Red line is a linear fit to the data.*

V. MEASUREMENTS

To ensure a reliable temperature accuracy and stability it is essential to demonstrate that there is no heating effect on the QD-PPMS by the high frequency excitation coil. We have measured the superconductor MgB_2, which has a superconducting critical temperature of 39 K, at 100 kHz and 1 MHz. Figure 6a shows the in-phase component of the diamagnetic susceptibility through the critical temperature and the determined transition is in agreement with literature for the extremes of the frequency range of the system at 100 kHz and 3 MHz. No imaginary part is observed because at the high frequencies and low amplitude (H_0=0.045 mT) of our system the peak is expected to be too narrow for the temperature step used[18] (1 K). A demagnetization correction has been applied such that $\chi'_V(T_{min}) = -1$, where $\chi'_V(T)$

is the in-phase component of the sample's volume ac-susceptibility at temperature T. Clearly the data are in agreement, demonstrating the acurracy and stability of the temperature with high frequency. Furthermore, the frequency dependent properties are checked by considering a sample of the spin ice $Dy_2Ti_2O_7$; the in- and out-of-phase component shown in figure 6b and c respectively were measured at 15 K using the ac susceptibility option (QD-ACMS) of the QD-PPMS. We can check the consistency of our system by overlaying the QD-ACMS data taken at similar frequencies to data taken using the coil set designed for this work and extending the data to higher frequency. The data show a clear overlap and demonstrate the accuracy of the equipment.

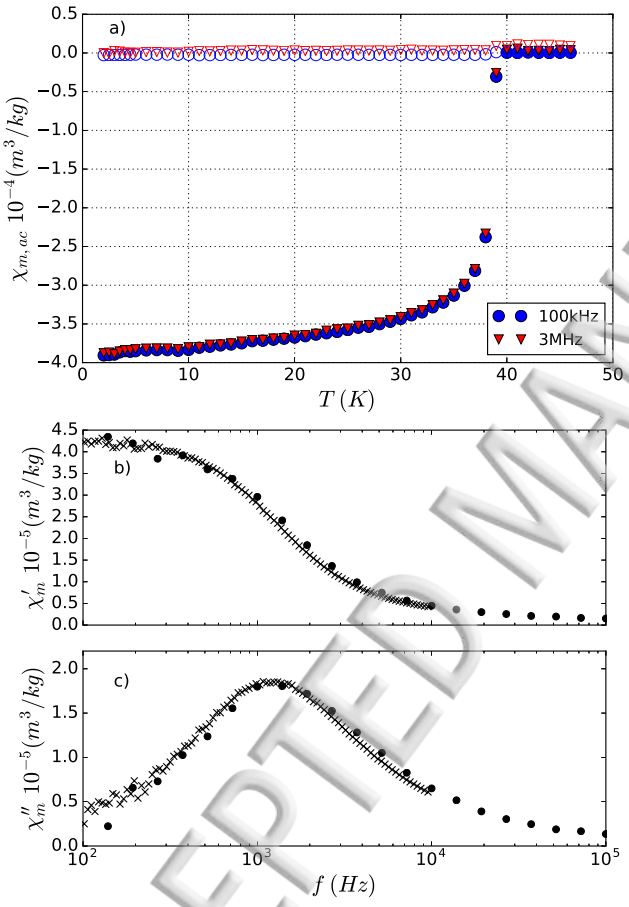

Figure 6: *Data to illustrate temperature accuracy. a) Mass ac-susceptibility vs. temperature on a powder MgB_2 for 100 kHz and 1 MHz through the superconducting transition of 39 K. Solid markers indicate the in-phase component and empty markers indicate the out-of-phase component. b) In-phase and c) out-of-phase mass ac-susceptibility on a single crystal of $Dy_2Ti_2O_7$ at 15 K. Dots indicate data taken by our high frequency set up and crosses indicate data taken by the QD-ACMS susceptometer.*

Data taken on two further samples are presented to illustrate the performance of the system at low and high temperatures. The first sample is $CdEr_2S_4$, which is a dipolar spin ice material with a spinel structure. Spin ices are materials in which geometric frustration on the crystal lattice causes novel magnetic behavior, including emergent quasi-particles and a residual entropy in the ground state[19]. High frequency susceptibility measurements on $CdEr_2S_4$ with the detailed in-phase and out-of-phase components shown in figure 7a and b were performed as part of a recent study into this material[20].

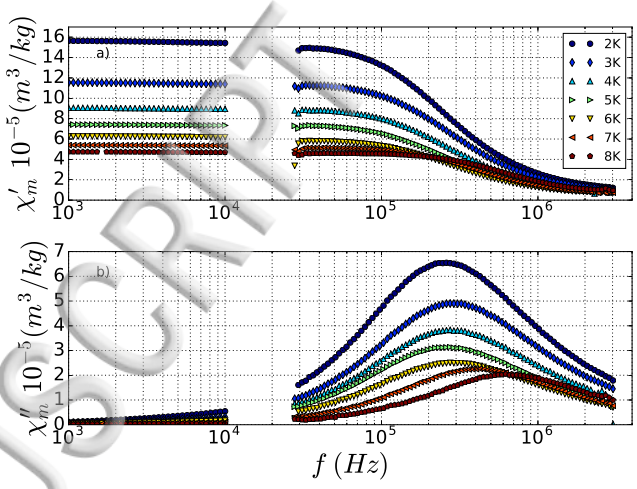

Figure 7: *Example of mass ac-susceptibility data vs. frequency of $CdEr_2S_4$ at low temperatures. a) the in-phase component and b) the out-of-phase component. Frequencies $< 10^4 Hz$ were measured by the QD-ACMS, frequencies $> 10^4 Hz$ were measured by our system.*

Magnetic nanoparticles can be used in biomedical applications such as magnetic particle imaging and magnetic fluid hyperthermia[21,22]. We measured an iron oxide based nanoparticle system produced by nanoPET Pharma GmbH, FeraSpin XS, which have a hydrodynamic particle diameter in the range 10-20 nm[23]. The peak in the imaginary part is expected to be broad[24], which allows us to illustrate the susceptometer measuring over a large temperature range.

The suspension liquid was frozen by cooling to 250 K at atmospheric pressure with zero applied field, then waiting for an hour before purging the sample chamber and cooling to measurement temperatures. The magnetic nanoparticles were measured at frequencies (f=31 kHz, 106 kHz, 363 kHz, 674 kHz and 1.25 MHz) across the temperature range 20-124 K and the result can be seen in figure 8. The maximum in-phase and out-of-phase components at a specific temperature, as shown in figure 8, are because the Néel relaxation time becomes similar to the measurement timescale.

An Arrhenius equation, which assumes coherent magnetization reversal in the magnetic core and non-interacting cores subject to small magnetic fields, was used to fit the determined peak temperatures at different relaxation times. For single core non-interacting nanoparticles this is a reasonable assumption[9]. The fitting equation is given by:

$$\tau(T) = \tau_0 \exp\left(\frac{KV}{k_B T}\right). \qquad (5)$$

This manuscript was accepted by Rev. Sci.Instrum. Click here to see the version of record.

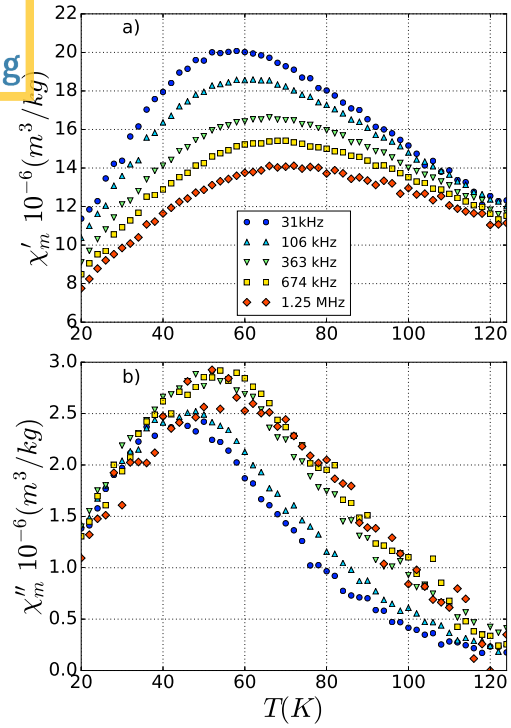

Figure 8: *Mass ac-susceptibiltiy data vs temperature for five frequencies of the FeraSpin XS magnetic nanoparticles. a) In-phase component. b) Out-of-phase component.*

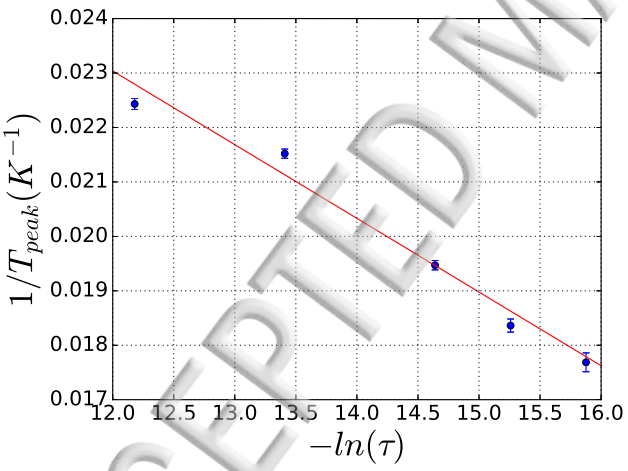

Figure 9: *Results of our analysis of the magnetic nanoparticle data in fig. 8 showing the inverse of the peak location in χ'' against the logarithm of the corresponding relaxation time for the relevant measurement frequency.*

where, τ_0 is often referred to as the attempt frequency and is usually in the range of 10^{-9} s and 10^{-10} s for iron oxide based nanoparticles, K is the magnetic anisotropy constant, V is the magnetic core volume and k_B is the Boltzmann constant. Figure 9 shows the inverse of the peak locations in temperature of $\chi''(T)$ against the corresponding intrinsic relaxation time associated with the measurement frequency according to $\tau = 1/2\pi f$. Peak locations and associated errors were estimated from Lorentzian fits to the data. By using the magnetic anisotropy constant suggested by Wetterskog *et. al.*[24] ($K = 2.8 \times 10^4 J/m^3$) for this nanoparticle system, we find the mean core diameter to be (8.86 ± 0.09) nm and $\tau_0 = (2.50 \pm 2.35) \times 10^{-13}$ s. Our Arrhenius analysis has found that τ_0 is of the same order of magnitude as estimated from the Arrhenius plot by Wetterskog *et. al.* The mean core diameter we find is slightly larger than reported by Wetterskog *et. al.* using transmission electron microscopy analysis (∼6 nm) but there is a good resemblance of the FeraSpin XS core diameter with recently reported data[25] using X-ray diffraction (XRD), neutron powder-diffraction (ND) and small angle x-ray scattering (SAXS), (∼9 nm). The different values of the core size can be due to different size weightings using different analysis techniques[25]. The slightly lower value of τ_0 can be due to magnetic interactions between the magnetic cores.

VI. SUMMARY

We have built an ac susceptometer capable of measuring the in-phase and out-of-phase ac susceptibilities at frequencies up to 3.5 MHz, across the temperature range 2-300 K, and in dc fields up to 9 T. This capability allows easy measurement of bulk samples in a range of temperatures, magnetic fields and frequencies previously very difficult to observe. Careful design of the coil winding has allowed us to minimize parasitic capacitance and inductance which, along with the calibration routines described, allow us to maintain stable precise measurements to high frequency with good sensitivity. We have reported on several example measurements performed on samples with different magnetic properties using the high frequency ac susceptometer illustrating its range and stability. Ac susceptibility measurements on MgB_2 and $Dy_2Ti_2O_7$ have shown that heating from the coil set is negligible and that the sample temperature is well known. Measurements performed on $CdEr_2S_4$ have demonstrated almost the full frequency range available and measurements on an iron oxide based magnetic nanoparticle system show functionality over a wide temperature range.

VII. ACKNOWLEDGEMENTS

SRG thanks ESPRC (EP/L019760/1 and EP/S016465/1) for funding. The authors would like to thank T. Fennell and O. Zaharko for samples. We would like to thank D. Billington for critical appraisal of our manuscript.

REFERENCES

[1] M. Nikolo. *American Journal of Physics*, 63(1):57–65, 1995.
[2] Dinesh Martien. Introduction to ac susceptibility. *Quantum Design*, 1994.

[3] C. V. Topping and S. J. Blundell. *J. Phys.: Condens. Matter*, 31(013001), 2019.
[4] H. C. Casimir, W. J. de Haas, and D. de Klerk. *Physica*, 6 (3):241–254, 1939.
[5] W. R. Abel, A. C. Anderson, and J. C. Wheatley. *Review of Scientific Instruments*, 35(4):444–449, 1964.
[6] E. H. Brandt. *Phys. Rev. B*, 58:6506–6522, Sep 1998.
[7] F. Ludwig, A. Guillaume, M. Schilling, N. Frickel, and A. M. Schmidt. *Journal of Applied Physics*, 108(3):033918, 2010.
[8] V. Cannella and J. A. Mydosh. *Phys. Rev. B*, 6:4220–4237, Dec 1972.
[9] S Bogren, A Fornara, F Ludwig, M del Puerto Morales, U Steinhoff, MF Hansen, O Kazakova, and C. Johansson. *International Journal of Molecular Sciences*, 16(9):20308–20325, 2015.
[10] F Ahrentorp, AP Astalan, C Jonasson, J Blomgren, B Qi, OT Mefford, M Yan, J Courtois, JF Berret, J Fresnais, et al. *AIP Conference Proceedings*, 1311(1):213–223, 2010.
[11] ED Dahlberg, M Hardiman, R Orbach, and J Souletie. *Physical Review Letters*, 42(6):401, 1979.
[12] RB Clover and WP Wolf. *Review of Scientific Instruments*, 41 (5):617–621, 1970.
[13] J Grambow and G Weber. *Journal of Physics E: Scientific Instruments*, 4(11):865, 1971.
[14] PC Fannin, BKP Scaife, and W Charles. *Journal of Physics E: Scientific Instruments*, 19(3):238, 1986.
[15] M Hanson and C Johansson. *Journal of Magnetism and Magnetic Materials*, 101(1-3):45–46, 1991.
[16] ST Boyd, V Kotsubo, R Cantor, A Theodorou, and JA Hall. *IEEE Transactions on Applied Superconductivity*, 19(3):697, 2009.
[17] D-X Chen, V Skumryev, and B Bozzo. *Review of Scientific Instruments*, 82(4):045112, 2011.
[18] M Ciszek, K Rogacki, K Oganisian, ND Zhigadlo, and J Karpinski. *The European Physical Journal B*, 78(3):359–365, 2010.
[19] AP Ramirez, A Hayashi, RJ al Cava, R Siddharthan, and BS Shastry. *Nature*, 399(6734):333, 1999.
[20] S Gao, O Zaharko, V Tsurkan, L Prodan, E Riordan, J Lago, B Fåk, AR Wildes, MM Koza, C Ritter, et al. *Physical Review Letters*, 120(13):137201, 2018.
[21] RM Ferguson, AP Khandhar, C Jonasson, J Blomgren, C Johansson, and KM Krishnan. *IEEE Transactions on Magnetics*, 49(7):3441–3444, 2013.
[22] QA Pankhurst, J Connolly, SK Jones, and JJ Dobson. *Journal of Physics D: Applied Physics*, 36(13):R167, 2003.
[23] Miltenyi Biotec GmbH. FeraSpin ™ Series : FeraSpin ™, 2011.
[24] E Wetterskog, A Castro, L Zeng, Sarunas Petronis, D Heinke, E Olsson, Lars Nilsson, N Gehrke, and Peter Svedlindh. *Nanoscale*, 9(12):4227–4235, 2017.
[25] P Bender, J Fock, MF Hansen, LK Bogart, P Southern, F Ludwig, F Wiekhorst, W Szczerba, LJ Zeng, D Heinke, et al. *Nanotechnology*, 29(42):425705, 2018.

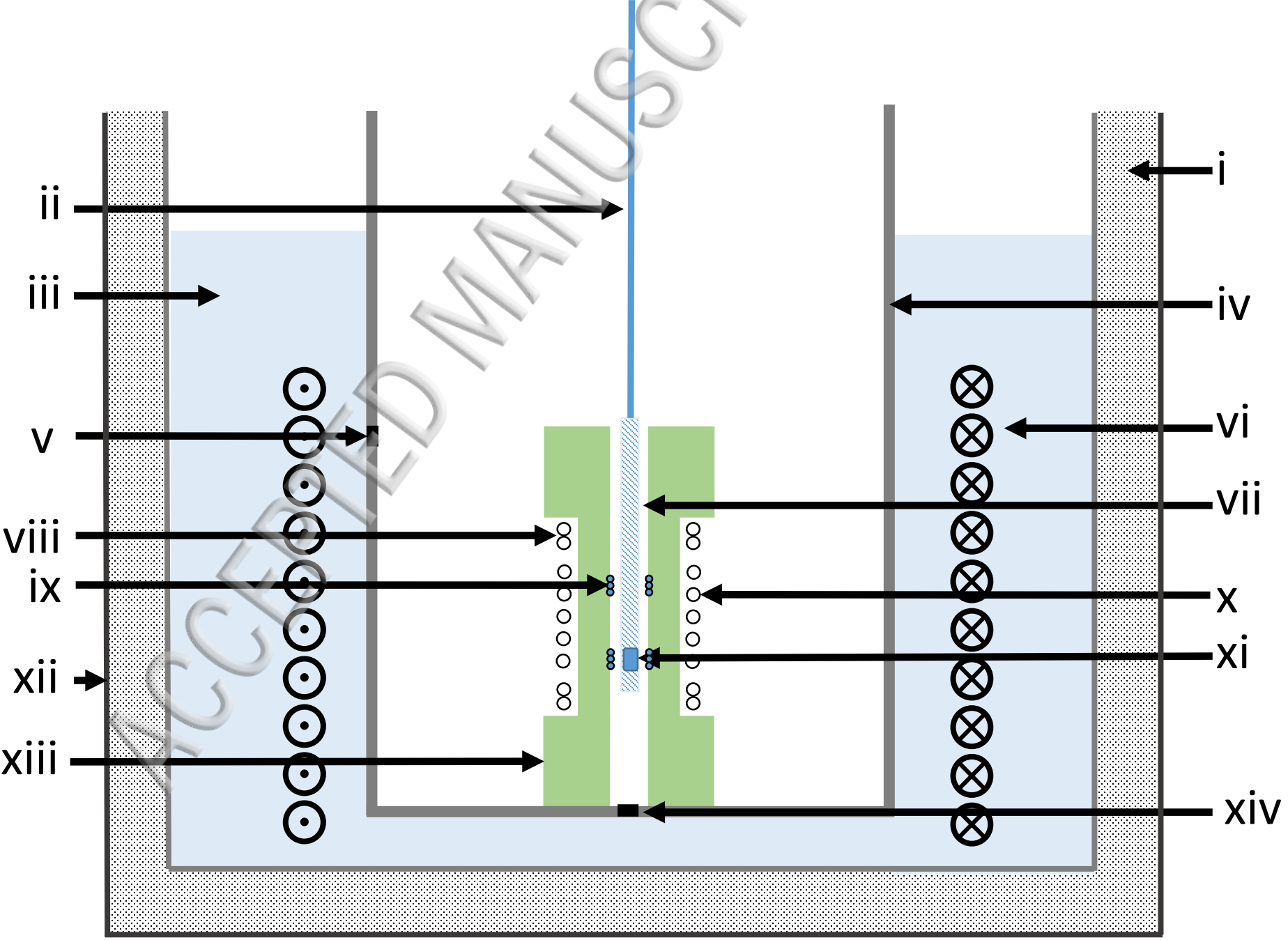

i. Vacuum jacket
ii. Actuator
iii. Helium bath
iv. VTI
v. Neck thermometer
vi. DC magnet coil
vii. Straw
viii. Shim coils
ix. Detection coils
x. Excitation coils
xi. Sample
xii. Shielding
xiii. Former
xiv. Base thermometer